BROOKHAVEN
NATIONAL LABORATORY

BNL-77188-2006-CP

Performance-limiting Defects in CdZnTe Detectors

A. E. Bolotnikov, *Member, IEEE*, G. S. Camarda, Y. Cui, K. T. Kohman, L. Li, *Senior Member, IEEE*, M. B. Salomon, and R. B. James, *Fellow, IEEE*

A. E. Bolotnikov, G. C. Camarda, Y. Cui, M. B. Salomon, and R. B. James are with Brookhaven National Laboratory, Upton, NY 11793
L. Li is with Yinnel Tech, Inc., 3702 West Sample Street, South Bend, Indiana 46619
K.T. Kohman is with Kansas State University, Manhattan, KS 66506

IEEE, Nuclear Science Symposium
San Diego, CA
October 29 – November 4, 2006

Nonproliferation and National Security Department
Detector Development and Testing Division

Brookhaven National Laboratory
P.O. Box 5000
Upton, NY 11973-5000
www.bnl.gov

DISCLAIMER

Performance-limiting Defects in CdZnTe Detectors

A. E. Bolotnikov, *Member, IEEE*, G. S. Camarda, Y. Cui, K. T. Kohman, L. Li, *Senior Member, IEEE*, M. B. Salomon, and R. B. James, *Fellow, IEEE*

***Abstract*—We studied the effects of small, <20 μm, Te inclusions on the energy resolution of CdZnTe gamma-ray detectors using a highly collimated X-ray beam and gamma-rays, and modeled them via a simplified geometrical approach. Previous reports demonstrated that Te inclusions of about a few microns in diameter degraded the charge-transport properties and uniformity of CdZnTe detectors. The goal of this work was to understand the extent to which randomly distributed Te-rich inclusions affect the energy resolution of CZT detectors, and to define new steps to overcome their deleterious effects. We used a phenomenological model, which depends on several adjustable parameters, to reproduce the experimentally measured effects of inclusions on energy resolution. We also were able to bound the *materials-related problem and predict the enhancement in* performance expected by reducing the size and number of Te inclusions within the crystals.**

***Index Terms*—CdZnTe, Te inclusions, semiconductor detectors.**

I. Introduction

UNTIL now, there has been no clear evidence that small, <20 μm, Te inclusions degrade the performance of CdZnTe (CZT) detectors more significantly that other factors (e.g., electronic noise, device geometry, and electron trapping) when a device's thickness exceeds several millimeters.

Grain boundaries, twins, or large Te inclusions size, >50 μm, are known to markedly worsen a device's performance [1-4]. However, the importance of small Te inclusions, <20 μm, has not been justified, because their influence on the efficiency of charge collection could not be measured directly with the mapping probes previously used (e.g., Refs. [4-8] and citations contained therein). The excitation areas of these was much wider (200-400 μm diameters) than the typical size of the Te inclusions. Optimistically, the inclusions were not considered to be harmful [9], at least in the case of thin detectors. On the other hand, the performance limitations of large volume, >1 cm^3, CZT detectors, even those made with the highest-quality single crystals suggest that the cumulative effects of a large number of them plays an important role.

Recently, we directly measured the charge trapped from the electron cloud by small individual Te inclusions [7,8]. These measurements were taken with a <10-μm diameter X-ray beam, and ~1-mm thick CZT samples, both of which factors were critical in enabling us to resolve individual inclusions and correlate their locations in X-ray maps and IR images. This work was in accord with results obtained from qualitative studies [4-6] revealing relationships between the concentration and shapes of Te inclusions, as identified in the material by IR transmission microscopy, and the devices' performances.

The goal of this study was to quantitatively analyze this effect and to demonstrate that it can explain the degradation of energy resolution and the losses in detection efficiency observed in CZT devices. Our practical goal was to estimate the extent to which the presence of Te inclusions can be tolerated. Accordingly, we measured the efficiency of charge collection with a highly collimated X-ray beam, and modeled electron transport in CZT devices containing Te inclusions.

II. Experimental Setup

Several experimental tools were employed to investigate the effects of small Te inclusions in detectors fabricated from CZT crystals grown by different techniques. The results from IR transmission microscopy were correlated with those obtained from the high spatial resolution X-ray mapping of thin, ~1 mm, CZT samples and pulse-height measurements of thick, 10-15 mm, samples configured as Frisch-ring detectors. Only high μτ-product, ~10^{-2} cm^2/V, crystals were selected for the measurements. Pulse-height spectra were acquired from uncollimated ^{137}Cs and ^{68}Ge sources. For time-resolved measurements (i.e., amplitude versus drift time), we employed a small, 3 cm^3, BaF_2 detector; 511-keV annihilation photons emitted by the ^{68}Ge source were used to produce coincidence signals in the CZT device and the BaF_2 detector [10]. Fast signals generated by the BaF_2 detector acted as triggers to locate the interaction moment of an incident photon.

A. X-ray mapping system

A new high-spatial resolution X-ray mapping system with a highly collimated monochromatic beam tunable in the range of 10-40 keV was recently commissioned at National Synchrotron Light Source, BNL to study CZT material and devices. We used it to measure variations in the charge collection efficiency over areas of the devices with <10-μm spatial resolution. We described the measurement procedure in detail elsewhere [11]. For each beam location, a pulse-height spectrum is collected, corresponding to the area of the detector

Manuscript received October 25, 2006.This work was supported by U.S. Department of Energy, Office of Nonproliferation Research and Engineering, NA-22. The manuscript has been authored by Brookhaven Science Associates, LLC under Contract No. DE-AC02-98CH1-886 with the U.S. Department of Energy.

A. E. Bolotnikov, G. C. Camarda, Y. Cui, M. B. Salomon, and R. B. James are with Brookhaven National Laboratory, Upton, NY 11793 USA (phone: 631-344-8014; e-mail: bolotnik@bnl.gov).

L. Li is with Yinnel Tech, Inc., 3702 West Sample Street, South Bend, Indiana 46619 USA.

K.T. Kohman is with Kansas State University, Manhattan, KS 66506 USA.

irradiated at the cathode side, and its peak position and width evaluated. The results are presented as 2 or 3D maps (X-ray maps) of the device's response. Fig. 1 shows a typical 2D image generated for 1x1 mm^2 area of 2-mm thick CZT detector. The pixel size is 10x10 μm^2, and X-ray energy is 30 keV. Dark spots clearly denote the Te inclusions. Fig. 2 plots the same data in 3D format, showing the deviations of the device's response from the average (depicted upside-down for clarity).

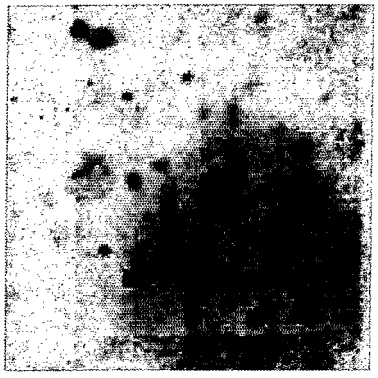

Fig. 1. Typical X-ray map generated for the 1x1 mm^2 area of a 2-mm thick CZT sample. The pixel size is 10x10 μm^2.

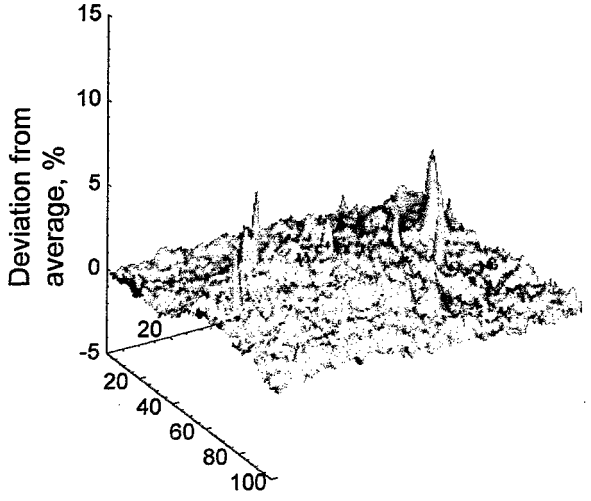

Fig. 2. 3D representation of the map shown in Fig. 1.

Collimated X-ray and alpha-particle beams normally are employed to screen internal defects in CZT material by measuring the amount of charge passed across a device. Free carriers are generated near the cathode, and the charge signal is detected at the anode. The amplitude and shape of output signals depend on defects in the path of the electron cloud. The minimum size of features that can be resolved with this mapping technique typically is limited by the size of the excitation areas which, in turn, is determined by a cross-section of a beam. However, when the size of a beam is below 100 μm, the spread of an electron cloud due to diffusion and electrostatic repulsion becomes a limiting factor. Calculations based on the solution of the drift-diffusion equation, which accounts for the mutual repulsion of electrons, predict a strong broadening of the electron cloud for alpha particles and gamma-rays [12,13]. Fig. 3 compares the evolution of the electron cloud's sizes (a sphere of 3-sigma diameter containing 99.73% of the electrons) generated by the 30-keV photoelectron and 5.5-MeV alpha particle. Initially, the electron cloud generated by the 5.5-MeV alpha particle is less than 25 μm, but quickly expands up to ~500-μm during the first 10 ns of the drift. These results indicate that alpha particles cannot successfully probe ~20 μm or smaller Te inclusions in CZT material, even in thin CZT samples and with highly collimated beams.

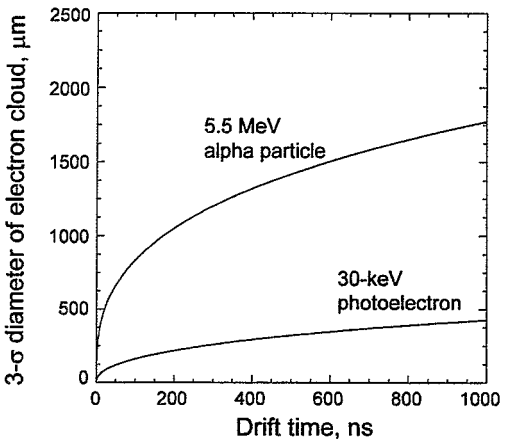

Fig. 3. Calculated 3-sigma diameter of the sphere containing 99.73% of the electrons from the electron cloud, generated by 5.5-MeV alpha particle and 30-keV photoelectron, versus the drift time.

Fig. 4 confirms this finding; it shows two raster scans we earlier simulated [13] for both types of probes, 30-keV X-rays (left), and 5.5-MeV alpha particles (right), used to excite a 1-mm thin CZT sample containing randomly distributed Te inclusions with effective diameters of 1-20 μm and a total concentration of 10^5 cm^{-3}. The 3-D and 2-D maps show 1x1 mm^2 areas scanned with 1-μm resolution (i.e., 1-μm step and beam sizes).

There is practical significance in the fact that the electron cloud expands rapidly to a size that depends primarily on the amount of the initially deposited charge. Thus, to resolve the effects of Te inclusions in X-ray scans, not only should samples preferably less than 1-mm thick be used, but also should low-energy X-rays (preferably less than 50 keV). Measurements taken with thin samples are less affected by diffusion, while employing the low-energy X-rays minimizes electrostatic repulsion. However, the energy of the X-ray beam should be high enough to ensure a high signal-to-noise ratio; an interval of 30-50 keV seems to be the most suitable for such measurements.

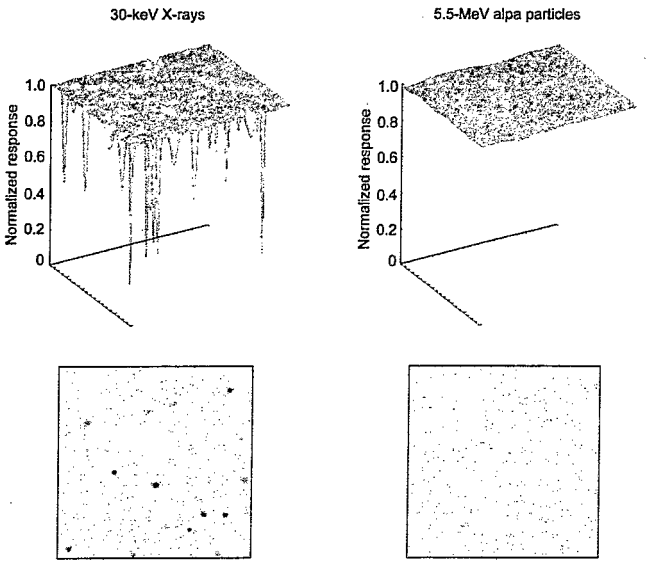

Fig. 4. Raster scans simulated for two types of probes: highly-collimated 30-keV X-ray (left), and 5.5-MeV alpha particle (right) beams. The scan's resolution is 1 μm, and its area is 1x1 mm^2. The X and Y axes represent the scan steps (1 μm) [13].

B. IR transmission microscopy

An automatic IR transmission microscope system was developed for screening internal defects in CZT samples. The system encompasses a large field-of-view microscope coupled with a 3.5-μm pixel size digital camera, a set of translation stages for positioning the samples, and a light illuminator. The digital camera provides 2208x3000 pixel images with a resolution of 0.19 and 0.75 μm per pixel depending on the lens' optical magnification. The important feature of this system is its iterative algorithm for counting Te inclusions and identifying their shapes and sizes [14]. Fig. 5 shows a fragment of the IR image with inclusions located in the focus automatically identified and circled.

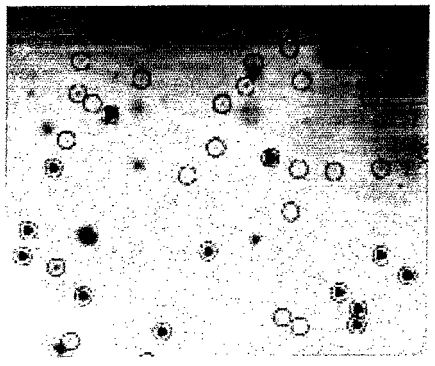

Fig. 5. A fragment of the IR image with the inclusions located in the focus automatically identified and circled.

Te inclusions are seen in IR images as 2D intensity distributions of regular or more often irregular shapes (depending on the inclusions' sizes and orientations) that result in uncertainties in determining their sizes. In our measurements, we define the precipitates' size (diameter) as 2.355σ, where σ is the standard deviation of the radius in the inclusion's intensity distribution. We estimated that the minimum size of Te inclusions distinguished above the noise with the IR system is ~0.5 μm, which are seen as much broader Gaussian-like intensity distributions. Consequently, the resolution of the IR system was insufficient for quantitative measurements of small inclusions, <1 μm. An etch pit technique would be better for measuring them.

III. Modeling Charge Loss Due to Inclusions

The number of trapped electrons depends upon the spread of the electron cloud that, in turn, is governed by the amount of the initially deposited charge and electron drift time. Gatti *et al.* first recognized the importance of electrostatic repulsion on the electron cloud's spread in semiconductor devices; they calculated the extent of this effect for Si drift detectors. [15]. Following their approach, we assessed the electron-cloud broadening in CZT material [12]; it predicts that for large deposited energies, electrostatic repulsion becomes the dominant effect thereby broadening the electron cloud. Moreover, this widening is practically independent of the initial distribution of the charge but is strongly tied to the total amount of deposited charge. In any case, the electron cloud becomes much larger than the size of the typical inclusion after drifting for the first 10 ns.

Let us first consider conventional electron trapping, i.e., the charge loss due to uniformly distributed impurity levels, so-called ordinary traps. Then, the decay of the charge is described by

$$Q = Q_0 \exp\left(-\frac{t_{drift}}{\tau_{bulk}}\right), \tag{1}$$

where Q and Q_0 are the collected- and initial-charge generated, t_{drift} is the electron cloud's drift time between the interaction point to the anode, and τ_{bulk} is defined as the electron's lifetime in the CZT bulk.

A similar approach can be taken to describe the charge loss due to an individual Te inclusion if the latter is considered as a microscopic region filled with a high concentration of ordinary traps:

$$Q = Q_i\left(1-\eta_i\left[1-\exp\left(-\frac{t_i}{\tau_i}\right)\right]\right), \tag{2}$$

where t_i and τ_i represent electron drift and lifetime, respectively, averaged over the geometrical region occupied by the i'th inclusion, and η_i is a fraction of charge from an electron cloud crossing the geometrical region of an inclusion. A difference between Equations (1) and (2) is that in the latter, Q_i represents the total amount of charge in the electron cloud right before passing the i'th inclusion. In other words, the

charge loss due to the interactions of an electron cloud with inclusions is a stochastic process. In addition, the ratio t_i/τ_i in Eq. (2) could differ from one inclusion to another.

Due to the lack of specific experimental details on the electron trapping mechanism by Te inclusions, we considered a simplified approach described in Refs. [12,13] that does not separately account for variations in local electric-fields, electron de-trapping, and extended areas of defects. Instead, it takes into account the overall effect by introducing a minimum number of free parameters that can be adjusted by data from experiments. Te inclusions are treated as geometrical spheres that punch holes in the electron cloud, which also is considered as a sphere with an electron distribution described by a three-dimensional Gaussian function.

With these assumptions, we can calculate, for the i'th inclusion, the fraction of electrons η_i happening to be within a footprint of the i'th inclusion of a certain effective diameter D_i. Thus, based on Eq. (2), the amount of charge left in the electron cloud after encountering a Te inclusion is

$$Q = Q_i\left(1-\eta_i\left[1-\exp\left(-\frac{D_i}{E_i\mu_i\tau_i}\right)\right]\right), \quad (3)$$

where the E_i is the local electric field-strength and $(\mu\tau)_i$-the product associated with the i'th inclusion. The product $(E\mu\tau)_i$ also can be called the inclusion's attenuation length λ_i. To reduce the number of free parameters, the attenuation length λ averaged over all inclusions can be used. In the simplest case, we assume that that all electrons from η_i get trapped (nontransparent inclusions), i.e.,

$$\frac{D_i}{E_i\mu_i\tau_i} >> 1. \quad (4)$$

Thus, the charge trapped by a Te inclusion depends on its effective diameter and its location with respect to the center of the electron cloud.

In the simulations, the electron clouds, generated by incident photons, were propagated through the crystal slab toward the anode in a constant electric field. In our idealized CZT detector, the output signals were determined as an amount of the collected charge. In other words, the reduction of the output signal was entirely due to charge trapped by randomly distributed Te inclusions. The original points of the interactions could be uniformly distributed over the cathode, which simulates the interactions of low-energy X-rays, or over the entire device's volume, which simulates the interactions of high-energy gamma rays, e.g., 662 keV.

We note that, currently, there are no experimental data to relate the effective and actual sizes of defect surrounding and within Te inclusions seen with an IR transmission microscope. If an extended area of defects surrounds an inclusion, this increases its apparent size. The same effect occurs if an inclusion accumulates positive space charge. In the case of a negative charge, field lines are deflected from an inclusion reducing its apparent size.

IV. Results and Discussion

A. Correlations between the size and concentration of Te inclusions and energy resolution

Spectral responses versus inclusion size/concentrations were measured for ~10 high-quality CZT samples configured as Frisch-ring detectors [16,17]. The samples were acquired from various vendors who used different crystal-growth techniques and post-growth annealing processes. Using the IR transmission microscope, the samples tested were classified in two classes: (1) those containing only small inclusions (<3 μm) with an average size in IR images (2.355σ) of ~1 μm, and, (2) those containing similar small inclusions, but also large ones (>5 μm) with an average size of >10 μm. In both cases, the total concentration of the IR visible inclusions was in the range 10^5-10^6 cm^{-3}.

With samples containing the small-sized inclusions, we measured the noise-subtracted energy resolution in the range 0.7-1.5% FWHM at 662 keV, e.g., 0.7% for a 4x4x11 mm^3 sample containing ~10^6 cm^{-3} IR visible inclusions, and 1.5% for 5x5x14 mm^3 sample containing ~3x10^6 cm^{-3} inclusions. Figs. 6(a) and 6(b), respectively, show the spectra measured for these samples. Since no correction for charge loss was applied, the broader peak measured for the 14-mm sample is primarily attributed to conventional electron trapping. Te inclusions with diameters of <3 μm, as seen with IR transmission microscopy, contribute < 1% to the total energy resolution at 662 keV in CZT detectors for thicknesses up to 15 mm at that concentration.

With large-sized inclusions, we clearly observed correlations between the degradation of the device's responses and size/concentration of Te inclusions. The details of these measurements will be reported elsewhere. Here, we provide two examples: an energy resolution of 1.1% FWHM at 662 keV was measured for a 5x5x11 mm^3 sample containing an average of ~5-μm inclusions with a concentration of ~3x10^5, and a value of 6.2% for a 6x6x12 mm^3 sample (Fig. 6(c)) containing an average of ~15-μm inclusions with a concentration of 1x10^5 cm^{-3}.

B. Results of modeling

Earlier, we gave a detailed description of the modeling of the cumulative effect of Te inclusions [12,13], where it was used to simulate alpha-particle and X-ray scans for thin CZT detectors containing Te inclusions. Here, we used a similar approach to model the spectral responses from long detectors, up to 20 mm, and compared them with those measured with the actual Frisch-ring detectors described in the previous section.

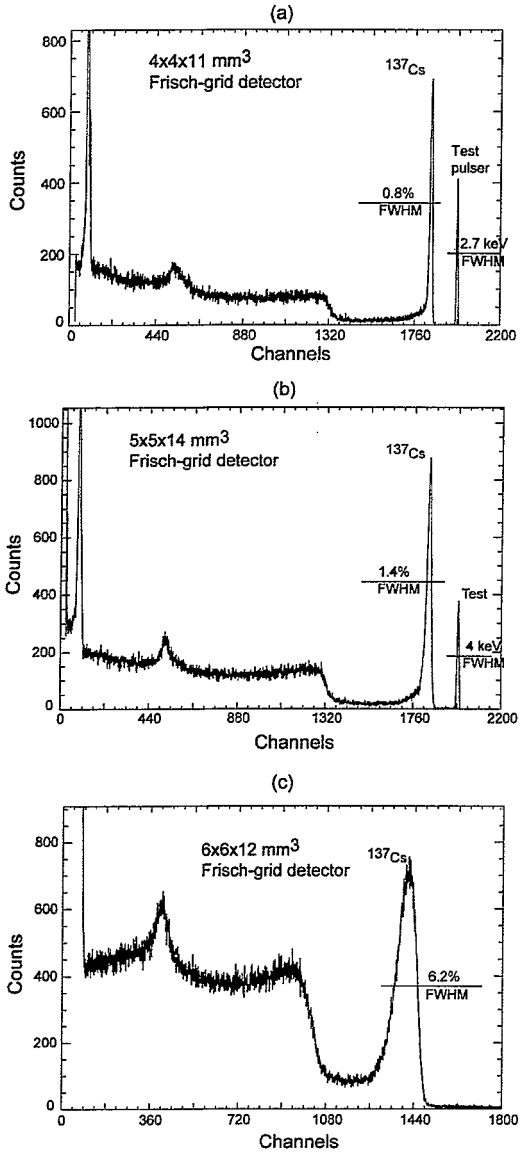

Fig. 6. Pulse-height spectra measured with CZT samples: (a,,b) 11- and 14-mm thick containing <3 μm inclusions with the concentration of ~10^6 cm^3, and, (c) 12-mm thick containing both small, <3 μm, and large, ~15 μm, inclusions.

In the simulations, we assumed an idealistic single-carrier device. In other words, the device's response (excluding factors such as electronic noise, charge trapping, and material non-uniformities) is represented by a delta-function regardless the locations of the interaction points. There are two real detectors whose responses approach the idealistic device; pixel and Frisch ring detectors.

To avoid time-consuming Monte Carlo simulations of the photons' transport and their energy dissipation, we generated the device's responses to unit charges randomly generated inside a small-area, 1x1 mm^2, but equal to the device's length voxel and then propagated them through the CZT crystal containing uniformly distributed inclusions. Then, we convolved the response function with the best ^{137}Cs pulse-height spectrum actually measured for the high-quality 4x4x11 mm^3 Frisch-ring detector (Fig. 6(a)). The width of the peak in this spectrum was artificially reduced down to 0.5%, to account for electronic noise, while the photo-peak's maximum was accordingly increased to maintain the original area beneath it. The results, presented below, were simulated for a 15-mm long device biased at 3000 V (The electric field strength is 2000 V/cm.).

First, we simulated the pulse-height spectrum assuming only the conventional electron-trapping process, $\mu\tau$=10^{-2} cm^2/V, without the effects of Te inclusions. Fig. 7 shows the modeled pulse-height spectra and the corresponding amplitude versus drift-time distributions (bi-parametric plot) before (top) and after (bottom) bi-parametric corrections. It shows that the original correlation curve (the dots concentrated along the line corresponding to the total energy-deposition events) has a slope due to electron trapping, although with a very narrow width. This signifies that conventional electron trapping can be straightforwardly corrected without loss in energy resolution.

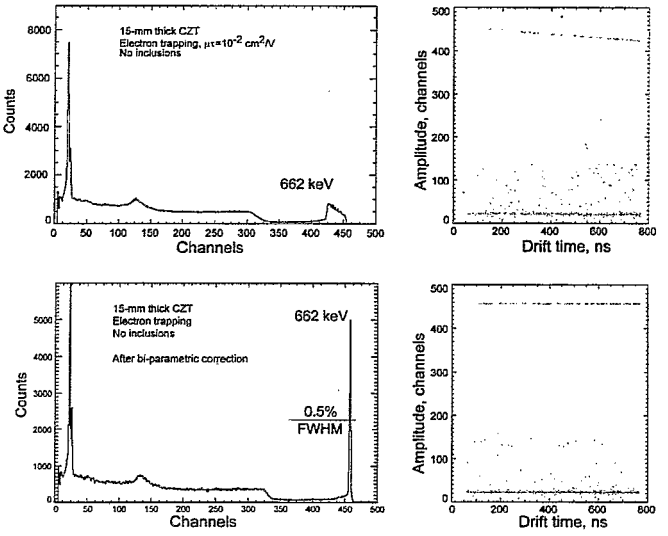

Fig. 7. Simulated pulse-height spectra and amplitude versus drift-time distributions (bi-parametric plot) before (top) and after (bottom) applying the bi-parametric correction. No inclusions are assumed; the $\mu\tau$-product is 10^{-2} cm^2/V.

Fig. 8 shows the spectra and bi-parametric distributions simulated for the sample containing 10-20μm inclusions with a concentration of 10^5 cm^{-3}. In addition to the slope representing conventional electron-trapping, the original correlation curve has much broader distribution compared with the previous case; this reflects additional fluctuations of the charge loss caused by the inclusions. Even though the slope of the correlation curve can be corrected, the remaining fluctuations still contribute to the peak's width (see the spectrum at the bottom). We note that the fluctuations caused by the Te inclusions were simulated for the 1x1x15 mm^3 voxel, and cannot be corrected even in high-granularity position sensitive detectors.

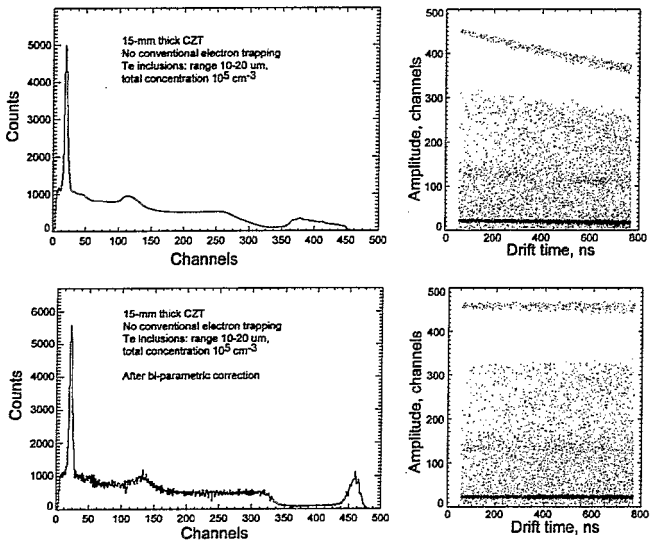

Fig. 8. Simulated pulse-height spectra and bi-parametric distributions for the sample containing 10-20-μm inclusions with a concentration of 10^5 cm^{-3} before (top) and after (bottom) applying the bi-parametric correction. No conventional electron trapping is assumed.

Fig. 9 shows a succession of curves representing the cumulative contribution, %FWHM at 662 keV, of the Te inclusions to energy resolution (after bi-parametric correction) versus their concentration calculated for 1-, 3-, 5-, 10-, and 20-μm inclusions. Again, the device's length was assumed to be 15 mm that is typical for thick CZT devices. As seen, the effect of the small-sized inclusions, <3 μm, becomes notable only at concentrations above 10^6-10^7 cm^{-3}, in a good agreement with the experimental results described above. On the other hand, the 1-μm inclusions show no effect whatsoever, meaning that Te inclusions of less than 1 μm behave almost as *regular traps*.

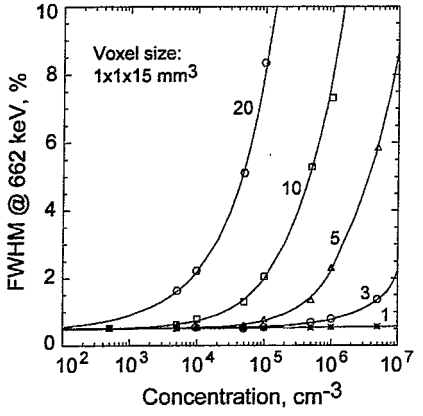

Fig. 9. Contribution, %FWHM at 662 keV, of the cumulative effect of Te inclusions to energy resolution (after bi-parametric correction) versus their concentration calculated for 1-, 3-, 5-, 10-, and 20-μm inclusions. The detector's length is 15 mm.

Using the data sets in Fig. 9, we evaluated the region in the parametric size-concentration space where the statistical fluctuations caused by Te inclusions contribute less than 0.5% FWHM at 662 keV (after bi-parametric correction) for a 15-mm long sample. The region below the solid curve shown in Fig. 10 corresponds to the sizes and concentrations of inclusions whose presence can be tolerated in CZT crystals up to 15-mm long used as radiation detectors.

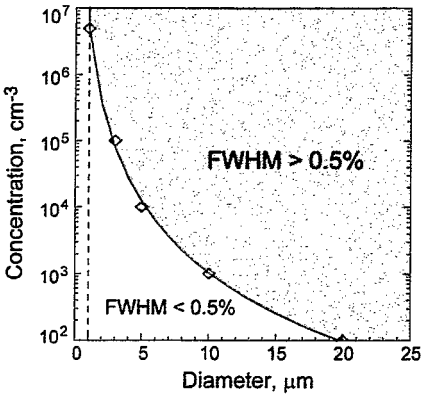

Fig. 10. Regions in two-parametric space where Te inclusions contribute to the peak's width greater (top) and less (bottom) than 0.5% FWHM at 662 keV.

However, for CZT crystal growers, the more important parameter is the total volume of extra Te present in the material. Assuming the inclusions are spherical the total volume they occupy can be easily estimated. Fig. 11 shows the same data given in Fig. 9 but plotted versus the percentage of the total volume of extra Te. In the first approximation, the dots evaluated for different size inclusions can be described by the same dependence (fitting curve in Fig. 11). Therefore, the maximum tolerable volume of extra Te located in inclusions (after bi-parametric correction and up to 15-mm long detectors) is ~$5x10^{-3}$ %.

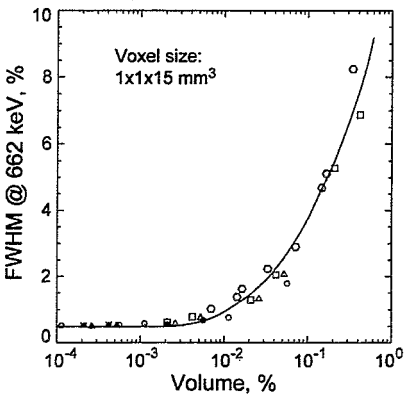

Fig. 11. Contribution of the cumulative effect of Te inclusions to energy resolution (the same data as in Fig. 9) versus percentage of the total volume of extra Te.

V. Conclusions

By combining the results obtained from IR transmission microscopy and radiation response measurements, we demonstrated a strong correlation between size of the inclusions and also of their concentration on the device's spectral response. These correlations were reproduced by applying a model that takes into account broadening of the electron cloud due to diffusion and electrostatic repulsion, and electron trapping by Te inclusions.

Both experimental measurements and simulations established close limits on the sizes and concentrations of Te inclusions that can be tolerated in CZT crystal devices.

Te inclusions of <1 μm behave as ordinary electron traps whose effect on the charge collection efficiency can be corrected. Inclusions of <3 μm can be tolerated up to concentrations of 10^6 cm^{-3} (after bi-parametric correction).

Depending on their concentration, Te inclusions with the sizes >3 μm may strongly degrade energy resolution in thick, >1 cm, detectors. In this case, the tolerable limit (threshold) can be expressed in terms of the percentage of the total volume occupied by extra Te, $<5x10^{-3}$ %.

The fluctuation in the charge loss, caused by these inclusions, cannot be corrected by depth sensing or similar techniques. This leaves only one option for resolving this problem, namely to produce CZT material with a reduced concentration and size of Te inclusions.

VI. Acknowledgment

The United States Government retains, and the publisher, by accepting the article for publication, acknowledges, a world-wide license to publish or reproduce the published form of this manuscript, or allow others to do so, for the United States Government purposes.

References

[1] J. R. Heffelfinger, D. L. Medlin, and R. B. James, "Analysis of Grain Boundaries, Twin Boundaries and Te Inclusions in Cadmium Zinc Telluride Grown by High-Pressure Bridgman Method", in Semiconductors for Room Temperature Radiation Detector Applications II, Vol. 487, edited by R. B. James, T. E. Schlesinger, P. Siffert, W. Dusi, M. R. Squillante, M. O'Connell and M. Cuzin (Materials Research Society, Pittsburgh, PA, 1998), p. 33.

[2] B. H. Parker, C. M. Stahle, S. D. Barthelmy, A. M. Parsons, J. Tueller, J. T. Van Sant, B. F. Munoz, S. J. Snodgrass, and R. E. Mullinix, "Correlation between bulk material defects and spectroscopic response in cadmium zinc telluride detectors," in Hard X-Ray, Gamma-Ray, and Neutron Detector Physics, edited by R. B. James and R. Schirato, eds., Proc. SPIE 3768, p. 129-137, 1999.

[3] B. H. Parker, C. M. Stahle, D. J. Roth, S. R. Babu, and J. Tueller, "Effect of twin boundaries on the spectroscopic performance of CdZnTe detectors," in Hard X-Ray and Gamma-Ray Detector Physics III, edited by R. B. James, Proc. SPIE 4508, p. 68-78, 2001.

[4] M. Amman, J. S. Lee, and P. N. Luke, "Electron trapping non-uniformity in high-pressure-Bridgman-grown CdZnTe", J. Appl. Phys., vol. 92 (6), pp. 3198-3206, 2002.

[5] C. Szeles, S. E. Cameron, J.-O. Ndap, and W. C. Chalmers, "Advances in the crystal growth of semi-insulating CdZnTe for radiation detector applications", IEEE Trans. Nucl. Sci., NS 49, n.5, pp. 2535-2540, 2002.

[6] V. Ivanov, L. Alekseeva, P. Dorogov, and A. Loutchanski, "Correlation between quality of CZT crystals and spectrometric performance of hemispherical radiation detectors", Proc. IEEE-RTSD, Rome 2004.

[7] G. A. Carini, A. E. Bolotnikov, G. S. Camarda, G. W. Wright, L. Li, and R. B. James, "Effect of Te inclusions on the performance of CdZnTe detectors", Appl. Phys. Lett. 88, p. 143515, 2006.

[8] G. S. Camarda, A. E. Bolotnikov, G. A. Carini, and R. B. James, "Effects of Tellurium Inclusions on charge collection in CZT Nuclear Radiation Detectors", in Countering Nuclear and Radiological Terrorism, edited by S. Aprkyan and D. Diamond, Springer, 2006, pp. 199-207.

[9] Paul N. Luke, Mark Amman, Julie S. Lee, "Factors affecting energy resolution of coplanar-grid CdZnTe detectors", IEEE Trans. Nucl. Sci. 51, n. 3, pp. 1199-1203, 2004.

[10] A. E. Bolotnikov, G. S. Camarda, G. A. Carini, M. Fiederle, L. Li, G. W. Wright, and R. B. James, "Performance Studies of CdZnTe Detector by Using a Pulse-Shape Analysis", Invited Paper, in Proceedings of SPIE Hard X-Ray and Gamma-Ray Detector Physics VII, edited by R. B. James, L. A. Franks, and A. Burger (SPIE, Bellingham, WA, 2005), 59200K-1, 59200K-12.

[11] G. A. Carini, A. E. Bolotnikov, G. S. Camarda, and R. B. James, "High-resolution x-ray mapping of CdZnTe detectors", submitted to Nucl. Instr. Meth., 2006.

[12] A. E. Bolotnikov, G. S. Camarda, G. A. Carini, Y. Cui, L. Li, and R. B. James, "Cumulative effects of Te inclusions in CdZnTe radiation detectors", submitted to Nucl. Instr. Meth. A, 2006.

[13] A. E. Bolotnikov, M. Black, G. S. Camarda, G. A. Carini, Y. Cui, K. T. Kohman, L. Li, M. Salomon and R. B. James, "The Effect of Te Precipitates on Characteristics of CdZnTe Detectors", in Proceedings of SPIE Hard X-Ray and Gamma-Ray Detector Physics VIII, Vol. 6319, edited by L. A. Franks, A. Burger, R. B. James, H. B. Barber, F. P. Doty, and H. Roehrig (SPIE, Bellingham, WA, 2006), 631903-1.

[14] G. S. Camarda, A. E. Bolotnikov, G. A. Carini, Y. Cui, K. T. Kohman, L. Li and R. B. James, "High Spatial-Resolution Imaging of Te Inclusions in CZT Material", in Proceedings of SPIE Hard X-Ray and Gamma-Ray Detector Physics VIII, Vol. 6319, edited by L. A. Franks, A. Burger, R. B. James, H. B. Barber, F. P. Doty, and H. Roehrig (SPIE, Bellingham, WA, 2006), 63190Z-1.

[15] E. Gatti, A. Longoni, P. Rehak, and M. Sampietro, "Dynamics of electrons in drift detectors", Nucl. Instr. Meth. A253, pp. 393-399, 1987.

[16] D. S. McGregor and R. A. Rojeski, U.S. Patent 6,175,120; issued Jan. 6, 2001.

[17] G. Montémont, M. Arques, L. Verger, J. Rustique, "A Capacitive Frisch Grid Structure for CdZnTe Detectors," IEEE Trans. Nucl. Sci. 48, pp. 278-281, 2001.